Observed Relationship between Tornado Intensity and Pretornadic Mesocyclone Characteristics

MICHAEL F. SESSA AND ROBERT J. TRAPP

Department of Atmospheric Sciences, University of Illinois at Urbana–Champaign, Urbana, Illinois

(Manuscript received 12 May 2019, in final form 6 December 2019)

ABSTRACT

In a previous study, idealized model simulations of supercell thunderstorms were used to demonstrate support of the hypothesis that *wide, intense tornadoes should form more readily out of wide, rotating updrafts.* Observational data were used herein to test the generality of this hypothesis, especially to tornado-bearing convective morphologies such as quasi-linear convective systems (QLCSs), and within environments such as those found in the southeastern United States during boreal spring and autumn. A new radar dataset was assembled that focuses explicitly on the *pretornadic* characteristics of the mesocyclone, such as width and differential velocity: the pretornadic focus allows us to eliminate the effects of the tornado itself on the mesocyclone characteristics. GR2Analyst was used to manually analyze 102 tornadic events during the period 27 April 2011–1 May 2019. The corresponding tornadoes had damage (EF) ratings ranging from EF0 to EF5, and all were within 100 km of a WSR-88D. A key finding is that the linear regression between the mean, pretornadic mesocyclone width and the EF rating of the corresponding tornado yields a coefficient of determination (R^2) value of 0.75. This linear relationship is higher for discrete (supercell) cases ($R^2 = 0.82$), and lower for QLCS cases ($R^2 = 0.37$). Overall, we have found that pretornadic mesocyclone width tends to be a persistent, relatively time-invariant characteristic that is a good predictor of potential tornado intensity. In contrast, the pretornadic mesocyclone intensity (differential velocity) tends to exhibit considerable time variability, and thus would offer less reliability in anticipating tornado intensity.

1. Introduction

Analyses of tornado occurrence show that strong to violent tornadoes cause a disproportionate amount of damage and fatalities (Ashley 2007). This is mainly due to the tendency for strong to violent tornadoes to have the widest and longest damage paths (Brooks 2004).

In an attempt to explain this relationship, Trapp et al. (2017, hereafter T17) posed the simple hypothesis that wide, intense tornadoes should form more readily from a contraction of wide mesocyclones or, equivalently, wide rotating updrafts. Support for this hypothesis was found in a set of idealized numerical simulations of supercell thunderstorms, which revealed robust linear correlations between updraft area and peak near-surface vertical vorticity (a proxy for tornado-like vortex strength). Updraft area itself was found to correlate most strongly with the low-level environmental vertical wind shear (see also Kirkpatrick et al. 2009; Trapp et al. 2018).

This hypothesis—and indeed the current study—is unconcerned with the specific details of the processes leading to tornadogenesis, for example, whether (and how) near-ground vertical rotation originates from a forward-flank region and/or rear-flank region, etc. (e.g., see Markowski and Richardson 2009; Trapp 2013; Davies-Jones 2015). However, as already noted, the T17 hypothesis does require that the tornado develop from a contraction of ''parent'' vertical vorticity, which is present over some surface-based depth. This parent vertical vorticity, which out of convenience is referred to as a mesocyclone, is necessarily represented herein as a Doppler velocity couplet in Doppler radar data (see section 2). Implicitly, the conceptual model underlying T17—and therefore also the present study—is that of a supercell, although as we will show, the tornado-generating storm need not be a supercell for T17's hypothesis to hold. Specifically, quasi-linear

Supplemental information related to this paper is available at the Journals Online website: https://doi.org/10.1175/WAF-D-19-0099.s1.

Corresponding author: Michael F. Sessa, msessa2@illinois.edu

DOI: 10.1175/WAF-D-19-0099.1

convective systems (QLCSs) are known to develop tornadoes from a contraction of a parent (meso) vortex (e.g., Trapp et al. 1999; Atkins et al. 2004) that can originate from supercell-like processes, such as the tilting of baroclinically generated horizontal vorticity (e.g., Trapp and Weisman 2003; Wheatley and Trapp 2008; Parker et al. 2019). QLCSs have also been shown (e.g., most recently by Conrad and Knupp 2019; see also Carbone 1983; Wheatley and Trapp 2008) to generate tornadoes through processes involving the release of a horizontal shearing instability (HSI). Even in these HSI-type cases, there is still a parent (miso) vortex that is contracted into the tornado (e.g., see Lee and Wilhelmson 1997). Thus, as in supercells, the pretornadic characteristics of these parent vortices should also exert a strong control on the eventual tornado intensity.

To help illustrate this, we recall that the physical basis for the T17 hypothesis is conservation of angular momentum, or equivalently, Kelvin's circulation theorem, which can be represented by

$$2\pi u_T r_T = \Gamma = 2\pi u_M r_M, \tag{1}$$

where r_T and u_T ($r_M$and u_M) are, respectively, the radius and tangential wind speed of the tornado (pretornadic mesocyclone), and Γ is circulation. T17 used the mesocyclone dataset of Trapp et al. (2005a) in Eq. (1) to demonstrate that a contraction of a large-r_M, weak-u_M mesocyclone more likely explains the existence of a large-r_T, strong-u_T tornado than does a small-r_M, strong-u_M mesocyclone. This is due to the fact that as r_M is reduced, the necessarily stronger u_M [through Eq. (1)] becomes implausibly high for pretornadic mesocyclonic rotational velocities, and even approaches the u_T of strong tornadoes.

One of the limitations of the Trapp et al. (2005a) dataset, and indeed of the larger and more comprehensive datasets of Smith et al. (2015) and Thompson et al. (2017), is that the diagnosed characteristics such as rotational velocity, differential velocity, and radius are of the mesocyclone while the tornado was in progress. In other words, the tornado characteristics are aliased onto those of the mesocyclone, implying that descriptions such as "clear and tight" (Thompson et al. 2017) refer at least in part to the tornado. This inclusion of the tornado was intentional in the studies of Smith et al. (2015) and Thompson et al. (2017), as well as in the more foundational study of Toth et al. (2013), who all sought to use *tornadic*-mesocyclone characteristics to help *diagnose* tornado intensity or damage rating. The objective of our study, on the other hand, is to use *pretornadic* mesocyclone characteristics to *predict* tornado intensity or damage rating, conditional on tornadogenesis. A dataset that can be used toward this end does not, to our knowledge, exist in the published literature beyond that of Davis and Parker (2014), who compiled a pretornadic mesocyclone dataset but did not expand their case selection outside of high shear, low convective available potential energy (CAPE) (HSLC) environments, and also did not reference an EF scale.

In section 2, the creation of a diverse mesocyclone dataset is described, as is the method employed to analyze the mesocyclone characteristics. The results of the analyses are presented in section 3, which show that observed intense tornadoes tend to form more readily out of wide mesocyclones within different convective modes and environments. A discussion of how these results might be applied in an operational setting is provided in section 4, followed by a summary and conclusions in section 5.

2. Methodology

Archived, single-site, WSR-88D Level II data of 102 tornadic events (Table 1) during the period from 27 April 2011 to 1 May 2019 were manually analyzed using the Gibson Ridge radar software (GR2Analyst). The events were selected to provide: seasonal and geographical diversity; a reasonable sample of parent-storm morphologies; a range of EF ratings, from EF0 to EF5 (20 EF0, 27 EF1, 24 EF2, 21 EF3, 6 EF4, 4 EF5); and variations in environmental conditions, including those characterized as HSLC as well as high shear, high CAPE (HSHC). Because of the desire to have access to polarimetric radar data to help confirm tornado presence (see below), the events were required to have occurred during approximately the past six years, excluding the EF5 cases. They were also required to have radar ranges less than 100 km throughout their lifetime in order to lessen the impact of radar range and beamwidth limitations (Wood and Brown 1997). In addition, no more than three events were selected from the same synoptic-scale system, and each tornado analyzed had to be the first produced by a storm: The former criterion was imposed as a compromise between the desire to maximize the number of events yet minimize similar and thus potentially dependent data; the later criterion was imposed to avoid potential confusion about how to classify a mesocyclone as "pretornadic" when in the presence of ongoing/dissipated tornadoes. Finally, any events with improperly dealiased Doppler velocities were excluded.

The parent-storm convective mode was characterized simply as discrete supercells (DSC), quasi-linear convective systems (QLCSs), or multicells (MUL) using

radar reflectivity data from the volume scan immediately prior to reported tornadogenesis. Following Trapp et al. (2005b) and Smith et al. (2012), a discrete storm was a relatively isolated entity with a single, high-reflectivity core (reflectivity $\geq$ 50 dBZ). A QLCS had contiguous reflectivity of at least 35 dBZ over a horizontal distance of at least 50 km, and a length-to-width aspect ratio of at least 3:1. If the parent storm did not meet the criteria of these two categories, it was typically a multicell storm or short line segment comprised of a more complex reflectivity structure including multiple reflectivity maxima in close proximity and thus was placed in the MUL category.

The primary analysis was of the pretornadic mesocyclone width, which was defined as the linear distance between velocity peaks in the vortex couplet. The latitude and longitude of the center of the gates of maximum velocity were used to calculate the linear distance. The presence of a mesocyclone itself was confirmed using a methodology similar to Smith et al. (2012). Specifically, we required a peak differential velocity (ΔV) $\geq 10\,\mathrm{m\,s^{-1}}$ over a horizontal distance of less than 7 km, over the depth of the three lowest radar elevation angles, during at least one volume scan. Each of the cases in this dataset was required to have met this threshold, regardless of their convective mode. The mesocyclone width, inbound and outbound velocity peaks, and ΔV were evaluated at the three lowest radar elevation angles, for up to four[1] volume scans (see Table 1) during the lifetime of the identifiable mesocyclone through the volume scan just prior to the time of reported tornadogenesis. The time of tornadogenesis was confirmed by a consideration and comparison of the NOAA Storm Events Database (NOAA/NCEI/NESDIS 2014) description of each tornado and the manual radar analysis (including evaluation of the possible presence of a tornado debris signature). The three elevation angles were 0.5°, 0.9°, and 1.3°, ±0.1° depending upon the specific radar site. Reflectivity and Doppler velocity images at each of the three elevation angles are shown for a high EF and a low EF DSC case at the time of the peak, mean (over the lowest three elevation angles), pretornadic width of the mesocyclone (Figs. 1 and 2). The apparent relationship shown in Figs. 1 and 2 between mesocyclone width and tornado EF scale was quantified for all cases using linear regression.

[1] Although some mesocyclones in our dataset had pretornadic lifetimes exceeding four volume scans (see Table 1), analysis of their characteristics beyond four volume scans did not provide unique information.

To further explore the relationship between tornado EF rating and mesocyclone width, and to build on previous efforts of using radar data to estimate tornado intensity (Toth et al. 2013; Kingfield and LaDue 2015; Thompson et al. 2017), an analysis of each tornadic circulation from the time of tornadogenesis through the time of dissipation was also completed. The first analysis time for each tornado was the first volume scan of the time of or after the time of tornadogenesis. Thus, the tornado was required to have a duration of at least one volume scan after tornadogenesis for the case to be included; because EF0 tornadoes tend to be particularly short lived, many EF0 cases initially considered for inclusion did not meet this criterion. The peak inbound and outbound velocities and the ΔV of the tornadic vortex were manually evaluated at the three lowest radar elevation angles of each volume scan throughout the life of the tornado. This analysis was used to determine if there was a relationship between the peak tornadic vortex strength (ΔV), EF rating, and peak pretornadic mesocyclone width of each storm.

3. Results

When all 102 cases were analyzed, higher EF-rated tornadoes tended to be associated with larger pretornadic mesocyclones (Fig. 3a), as quantified by a coefficient of determination (R^2) of 0.75 in the linear regression between these two variables. This linear relationship is based on the use of total average mesocyclone width, defined as the mean mesocyclone width over the lowest three elevation angles and all volume scans analyzed during the pretornadic period. When the maximum estimated tornadic wind speed from damage assessments, collected from the NWS Damage Assessment Toolkit, is used in place of EF rating (see also Cohen et al. 2018), the strong linear relationship between higher damage rated tornadoes and the total average mesocyclone width remains (R^2 = 0.77; Fig. S1 in the online supplemental material). The linear relationship is slightly stronger when only the cases meeting the DSC mode classification (49 cases) were analyzed (Fig. 3b, R^2 = 0.82), and weaker when only the cases meeting the QLCS mode classification (39 cases) and MUL mode classification (14 cases) were analyzed (Fig. 3c, R^2 = 0.37 and Fig. 3d, R^2 = 0.38). This may be due to the fact that the QLCS (and MUL) cases had relatively shorter-lived and weaker pretornadic mesocyclones and tornadoes (see Table 1).

The regression analyses are supported by box-and-whisker plots, which show a distinct separation between the pretornadic mesocyclone widths for relatively

TABLE 1. List of all cases included in this study with the location and time of resultant tornadogenesis. In the last column, "total volume scans" indicates the number of pretornadic radar volume scans analyzed to determine the pretornadic mesocyclone characteristics. This number is bolded for cases in which there were more than four volume scans meeting the differential velocity threshold.

State	County	Date	Time (UTC)	EF rating	Mode	WSR-88D location	Tornadogenesis latitude, longitude	Tornadogenesis radar range (km) and 0.5° beam height (m)	Total volume scans
Alabama	Dekalb	21 Feb 2014	0628	2	QLCS	KHTX	34.49098°, −85.68685°	60.3, 784.8	4
Alabama	Lee	29 Apr 2014	0857	3	MUL	KMXX	32.48257°, −85.22983°	52.3, 593.7	4
Alabama	Marion	13 Oct 2014	2143	0	DSC	KGWX	34.16820°, −88.20008°	34, 362	2
Alabama	Washington	17 Nov 2014	0737	1	QLCS	KMOB	31.44722°, −88.16686°	84.9, 1289.5	4
Alabama	Jefferson	25 Dec 2015	2258	2	DSC	KBMX	33.442162°, −86.927582°	32.3, 321.2	4
Alabama	Russell	16 Feb 2016	0057	1	QLCS	KMXX	32.393913°, −85.353882°	43.8, 470.8	4
Alabama	Jefferson	1 Mar 2016	2343	2	QLCS	KBMX	33.327026°, −86.977173°	25.3, 240.4	4
Alabama	Dekalb	30 Nov 2016	0600	3	DSC	KHTX	34.729218°, −85.703407°	37.1, 431.2	4
Alabama	Morgan	30 Nov 2016	0240	3	DSC	KHTX	34.480186°, −87.089828°	80, 1133.4	4
Alabama	Cullman	29 Apr 2014	0239	3	DSC	KHTX	34.128632°, −86.746483°	100, 1384.3	4
Alabama	Etowah	29 Apr 2014	0532	3	DSC	KHTX	34.167267°, −86.063339°	85.3, 1232.8	4
Alabama	Blount	20 Mar 2018	0050	1	DSC	KHTX	33.866283°, −86.394547°	31.5, 320	4
Alabama	Crenshaw	22 Apr 2018	1843	1	MUL	KEOX	31.747765°, −86.413589°	48.1, 582.7	**4**
Alabama	Baldwin	22 Apr 2018	2025	0	DSC	KMOB	30.366745°, −87.679688°	54.8, 687.2	2
Alabama	Pickens	31 Aug 2017	2040	2	DSC	KGWX	33.305309°, −88.088593°	35.5, 358.7	4
Alabama	Montgomery	7 Apr 2016	0355	0	MUL	KMXX	32.296135°, −86.248001°	19.3, 201.1	2
Alabama	Bullock	7 Apr 2016	0454	2	QLCS	KMXX	32.133884°, −85.544609°	81.2, 1064.3	**4**
Alabama	Perry	14 Mar 2019	2319	0	DSC	KBMX	32.76424°, −87.350746°	81.7, 1162.7	**4**
Arkansas	Crawford	24 Mar 2016	0254	2	MUL	KSRX	35.744713°, −94.488205°	35.3, 363.3	**4**
Arkansas	Saline	25 Mar 2017	0333	2	QLCS	KLZK	34.535961°, −92.776123°	94.5, 1301.1	4
Arkansas	Crawford	28 May 2017	0456	1	MUL	KSRX	35.614834°, −94.357018°	88.2, 1191.7	4
Arkansas	Faulkner	28 Apr 2014	0025	4	DSC	KSRX	34.846554°, −92.545464°	57.5, 681.4	4
Arkansas	Franklin	3 May 2018	1809	1	QLCS	KSRX	35.335468°, −93.995399°	63.7, 750.6	3
Arkansas	Franklin	27 Apr 2016	0618	0	QLCS	KSRX	35.516239°, −93.928238°	34.9, 351.4	2
Florida	Calhoun	17 Nov 2014	1017	2	DSC	KEVX	30.408609°, −85.067505°	83.7, 1149.3	4
Florida	Escambia	15 Feb 2016	2132	3	DSC	KMOB	30.870422°, −87.379295°	98.9, 1375.8	4
Florida	Okeechobee	6 Apr 2017	1351	2	DSC	KMLB	27.58659°, −81.065308°	92.4, 1284.9	3
Florida	Brevard	13 Sep 2016	1751	0	DSC	KMLB	27.865786°, −80.547989°	79.5, 1120.9	**4**
Florida	Leon	19 Apr 2015	1651	1	QLCS	KTLH	30.501642°, −84.311531°	96.1, 1320.6	1
Florida	Wakulla	4 Mar 2019	0106	0	QLCS	KTLH	30.223423°, −84.607841°	68, 903.9	3
Georgia	Fulton	13 Oct 2014	0920	0	QLCS	KFFC	33.690361°, −84.461899°	50.4, 575.7	4
Georgia	Laurens	21 Feb 2014	1321	2	QLCS	KJGX	32.578373°, −82.965683°	66.2, 818.6	4
Georgia	Chattahoochee	23 Nov 2014	2037	1	QLCS	KMXX	32.334404°, −84.787971°	40.8, 443.4	4
Georgia	Bacon	4 Jan 2015	1808	1	QLCS	KVAX	31.529169°, −82.422798°	83.8, 1088.6	4
Georgia	Calhoun	7 Apr 2016	0645	2	MUL	KEOX	31.625446°, −84.882278°	68.7, 939.3	4
Georgia	Thomas	22 Jan 2017	0835	2	DSC	KTLH	30.917221°, −83.97538°	89, 1202	2
Georgia	Laurens	5 Apr 2017	1938	2	QLCS	KJGX	32.337814°, −82.975868°	49.6, 569	3

TABLE 1. (*Continued*)

State	County	Date	Time (UTC)	EF rating	Mode	WSR-88D location	Tornadogenesis latitude, longitude	Tornadogenesis radar range (km) and 0.5° beam height (m)	Total volume scans
Georgia	Houston	1 Apr 2016	1142	1	QLCS	KJGX	32.618191°, −83.687416°	22.1, 217.9	4
Georgia	Burke	19 Apr 2015	1942	2	QLCS	KCAE	33.22802°, −81.954544°	43.9, 498	**4**
Georgia	Bibb	7 Nov 2018	2235	0	QLCS	KJGX	32.733166°, −83.739098°	82, 1041.7	2
Illinois	Grundy	23 Jun 2015	0245	3	QLCS	KLOT	41.297737°, −88.350349°	57, 663.5	4
Illinois	Lee	9 Apr 2015	2339	4	DSC	KLOT	41.860466°, −89.254776°	92.8, 1376.4	4
Illinois	Macon	1 Dec 2018	2353	1	DSC	KILX	39.768291°, −89.102203°	82.8, 1096.6	2
Illinois	Mason	1 Dec 2018	2253	1	DSC	KILX	40.215126°, −89.945953°	61.7, 651	**4**
Iowa	Guthrie	8 Oct 2018	2322	0	QLCS	KDMX	41.802029°, −94.398979°	28.2, 280.7	3
Iowa	Dallas	20 Jun 2018	1918	0	DSC	KDMX	41.827671°, −94.158234°	11.8, 123.7	3
Kansas	Greenwood	27 Jun 2018	0018	3	DSC	KICT	37.834129°, −96.268356°	50, 530.6	4
Kansas	Pawnee	17 May 2017	0059	3	DSC	KDDC	38.195774°, −99.03035°	31.3, 314.5	**4**
Kansas	Ottawa	26 May 2016	0007	4	DSC	KTWX	38.985374°, −97.460312°	103.7, 1612	**4**
Kansas	Greenwood	8 Jul 2016	0210	3	DSC	KICT	37.969761°, −96.454147°	92.6, 1296.5	4
Kansas	Sedgwick	6 May 2015	2149	3	DSC	KICT	37.834003°, −97.642754°	61.1, 655.2	4
Kansas	Rice	13 Jul 2015	2334	3	DSC	KICT	38.182598°, −98.003372°	59.4, 761.6	4
Kansas	Comanche	5 May 2007	0200	5	DSC	KDDC	37.333546°, −99.475868°	48.1, 528.1	**4**
Kansas	Gray	29 May 2018	2144	0	DSC	KDDC	37.667858°, −100.28627°	47.2, 515.6	3
Kentucky	Graves	10 May 2016	1944	3	DSC	KPAH	36.758736°, −88.70507°	50.3, 576.6	**4**
Kentucky	Oldham	12 Apr 2019	10:45	1	Other	KLVX	38.324356°, −85.522881°	16.7, 155.1	2
Louisiana	Orleans	7 Feb 2017	1712	3	DSC	KLIX	30.01432°, −89.988319°	84.5, 1087.4	4
Louisiana	Ascension	7 Feb 2017	1700	1	DSC	KLIX	30.111538°, −91.040474°	54.2, 610.4	4
Louisiana	Bienville	14 Apr 2018	0647	2	QLCS	KSHV	32.456539°, −92.891983°	60.7, 730.5	2
Louisiana	Beauregard	7 Apr 2018	0617	1	QLCS	KPOE	30.83827°, −93.41082°	58, 661.3	4
Louisiana	Acadia	29 Aug 2017	2209	2	MUL	KLCH	30.242975°, −92.580864°	32.8, 328.5	**4**
Louisiana	Beauregard	12 May 2017	0906	1	MUL	KLCH	30.573786°, −93.570755°	43, 497.7	3
Louisiana	Rapides	1 Nov 2018	0525	1	QLCS	KPOE	31.206945°, −92.576675°	98.5, 1502.8	4
Michigan	Antrim	28 Aug 2018	2349	0	QLCS	KAPX	44.943069°, −84.973412°	49.5, 530	3
Minnesota	Rice	20 Sep 2018	2346	0	QLCS	KMPX	44.408062°, −93.273529°	81.4, 1066.4	2
Mississippi	Winston	28 Apr 2014	2147	4	DSC	KLIX	32.893356°, −89.444901°	18.8, 177.3	4
Mississippi	Marion	23 Dec 2014	2020	3	QLCS	KLIX	31.167202°, −89.917427°	32.4, 336.4	4
Mississippi	Marshall	23 Dec 2015	2212	4	DSC	KMPX	34.573166°, −89.762703°	99.8, 1430.6	4
Mississippi	Forrest	21 Jan 2017	0947	3	DSC	KLIX	31.196732°, −89.502884°	92.4, 1241.9	4
Mississippi	Prentiss	31 Aug 2017	1843	0	DSC	KGWX	34.419193°, −88.529869°	97.9, 1384.6	4
Mississippi	Yazoo	30 Apr 2017	1354	2	MUL	KDGX	32.649696°, −90.317909°	90.8, 1238.9	4
Mississippi	Covington	2 Jan 2017	2021	2	QLCS	KDGX	31.711102°, −89.723709°	27.7, 331.6	4
Mississippi	Scott	21 Jan 2016	2346	0	QLCS	KDGX	32.261646°, −89.527664°	72.4, 1052.1	4
Mississippi	Yazoo	30 Apr 2017	1354	2	QLCS	KDGX	32.653996°, −90.310333°	38.7, 378.5	4
Mississippi	Monroe	25 May 2015	1351	1	QLCS	KGWX	33.981628°, −88.537033°	94.1, 1308.4	4
Mississippi	Neshoba	27 Apr 2011	1930	5	DSC	KDGX	32.805496°, −89.109093°	34.5, 395.9	**4**
Mississippi	Scott	18 Apr 2019	2042	1	QLCS	KDGX	32.560276°, −89.77832°	26.7, 284.6	2

TABLE 1. (*Continued*)

State	County	Date	Time (UTC)	EF rating	Mode	WSR-88D location	Tornadogenesis latitude, longitude	Tornadogenesis radar range (km) and 0.5° beam height (m)	Total volume scans
Mississippi	Scott	1 Nov 2018	0920	1	QLCS	KDGX	32.433239°, −89.712395°	75.6, 968.6	2
Missouri	Newton	22 May 2011	2234	5	DSC	KSGF	37.05542°, −94.547821°	96.7, 1442.8	4
Missouri	Stone	1 May 2019	0135	1	QLCS	KSGF	36.809959°, −93.52935°	61.3, 755.2	4
N. Carolina	Beaufort	25 Apr 2014	2335	3	DSC	KRAX	35.535633°, −77.134506°	47.4, 569.9	**4**
N. Carolina	Nash	19 Apr 2019	2208	1	QLCS	KRAX	36.000507°, −77.817673°	23.5, 231.6	2
Ohio	Clark	7 Feb 2019	2017	0	QLCS	KILN	39.837982°, −83.77195°	69.9, 878.3	3
Oklahoma	Garvin	9 May 2016	2106	4	DSC	KTLX	34.551369°, −97.347679°	37.9, 405	4
Oklahoma	Oklahoma	7 May 2015	0141	3	DSC	KTLX	35.41383°, −97.488762°	51.4, 591.2	3
Oklahoma	Cleveland	20 May 2013	2004	5	DSC	KTLX	35.282242°, −97.629356°	68.5, 862.5	4
Oklahoma	Wagoner	30 Apr 2019	2002	1	DSC	KINX	35.99704°, −95.453094°	24.7, 244.4	4
Oklahoma	Mayes	19 Aug 2018	2045	1	DSC	KINX	36.079399°, −95.431885°	46.1, 515.3	4
S. Carolina	Aiken	19 Apr 2015	2010	2	QLCS	KCAE	33.514923°, −81.730881°	43.5, 479.4	4
S. Carolina	Charleston	25 Sep 2015	0442	2	DSC	KCLX	32.720291°, −80.057617°	49.5, 563.8	4
S. Carolina	Pickens	8 Oct 2017	2040	2	MUL	KGSP	34.776901°, −82.76239°	31.2, 322.1	4
S. Carolina	Spartanburg	23 Oct 2017	1912	2	QLCS	KGSP	34.975124°, −81.983238°	51.8, 597	4
S. Carolina	Horry	24 Oct 2017	0227	1	MUL	KLTX	33.836575°, −78.906372°	34.4, 360.8	4
S. Carolina	Saluda	24 May 2017	1904	2	MUL	KCAE	34.107128°, −81.640121°	37, 393.1	3
S. Carolina	Richland	11 Oct 2018	0822	0	DSC	KCAE	33.785206°, −80.671425°	42.8, 470.2	4
S. Carolina	Orangeburg	11 Oct 2018	0348	0	DSC	KCAE	33.488239°, −80.897774°	51.8, 596.1	**4**
Tennessee	Clairborne	27 Jul 2014	2159	3	DSC	KMRX	36.463909°, −83.977249°	56.3, 662.6	4
Tennessee	Polk	30 Nov 2016	0728	3	DSC	KHTX	35.118511°, −84.772736°	55.4, 649.8	4
Tennessee	Hickman	28 Jun 2018	1736	1	MUL	KOHX	35.726044°, −87.316063°	18.9, 181.6	3
Tennessee	Humphreys	6 Jul 2017	0158	0	QLCS	KOHX	36.158947°, −87.682045°	16, 150.8	4
Tennessee	Grundy	6 Nov 2018	0739	1	QLCS	KHTX	35.381592°, −85.81694°	36.3, 366	2
Texas	Eastland	9 May 2015	2132	3	DSC	KDYX	32.302097°, −99.004395°	26.5, 266.3	4

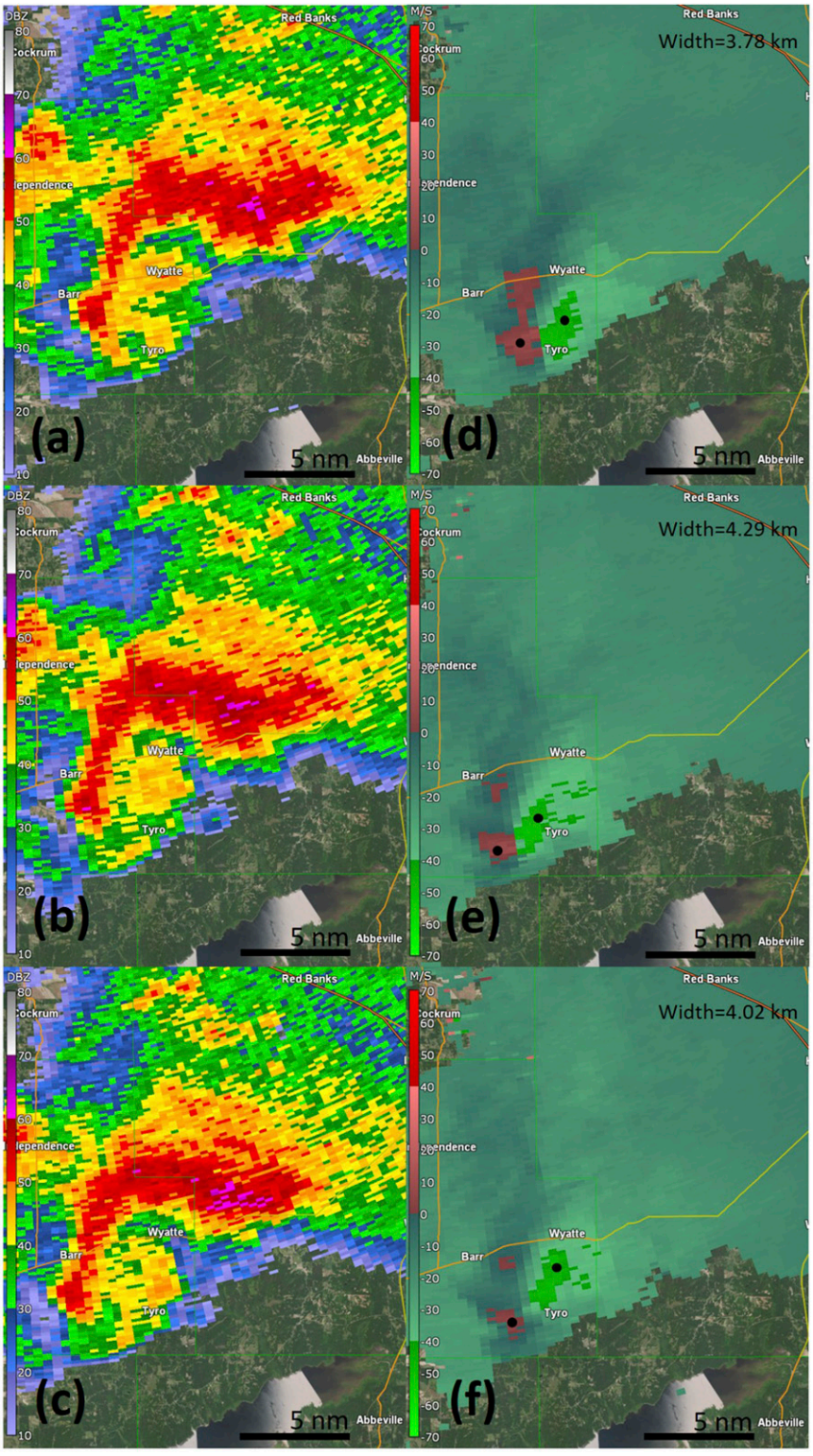

FIG. 1. (a)–(c) Radar reflectivity factor (dBZ) and (d)–(f) storm relative Doppler velocity (m s^{-1}) at the 0.5°, 0.9°, and 1.3° elevation angles, for the pretornadic supercell associated with the Marshall, Mississippi, EF4 tornado at 2207 UTC 23 Dec 2015. The distance from the radar was approximately 70 km and the 0.5° beam height was approximately 1121 m. This is the time of the peak total average mesocyclone width.

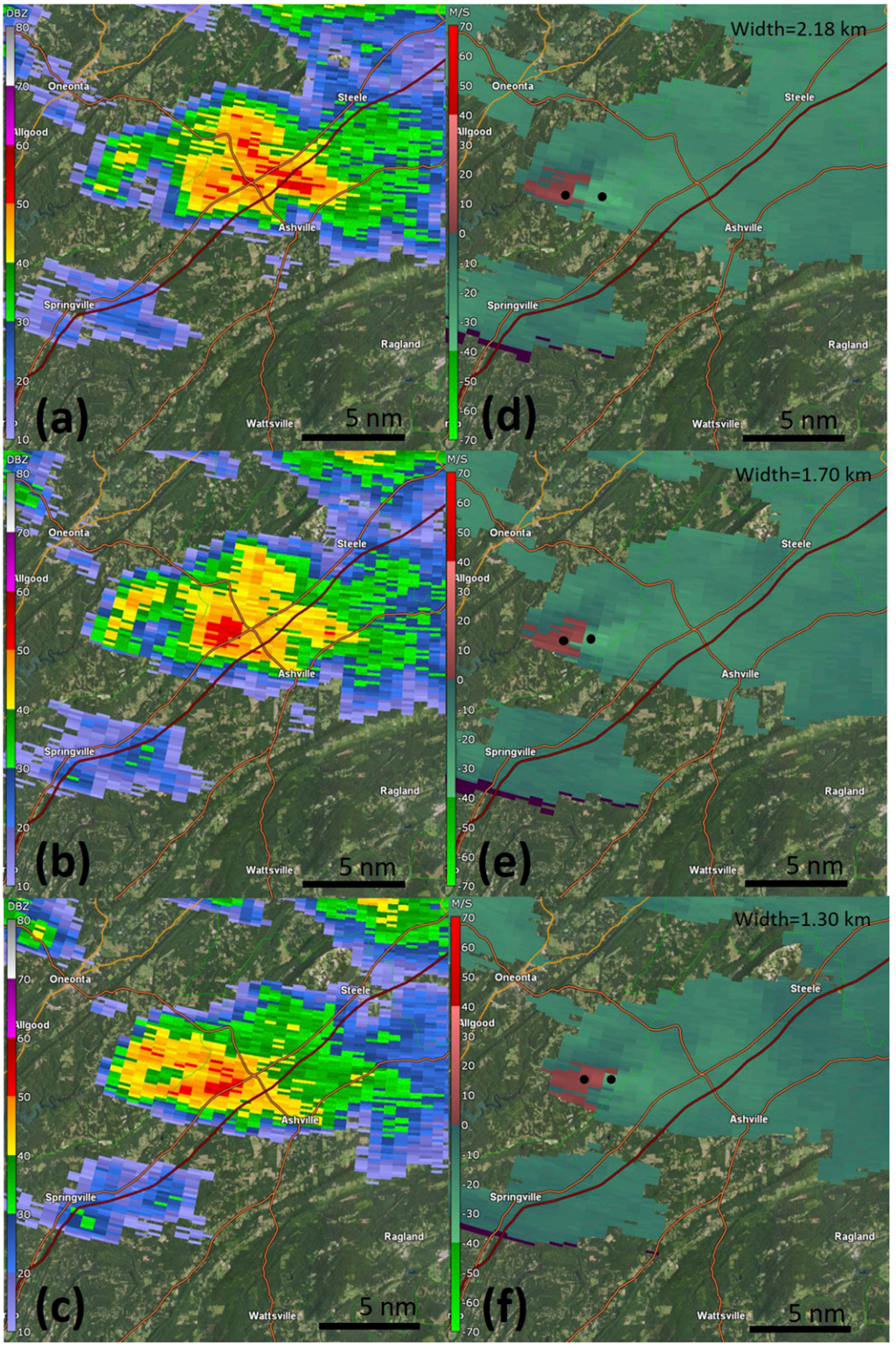

FIG. 2. As in Fig. 1, but for the pretornadic supercell associated with the Blount, Alabama, EF1 tornado at 0042 UTC 20 Mar 2018. The distance from the radar was approximately 82 km and the 0.5° beam height was approximately 1042 m.

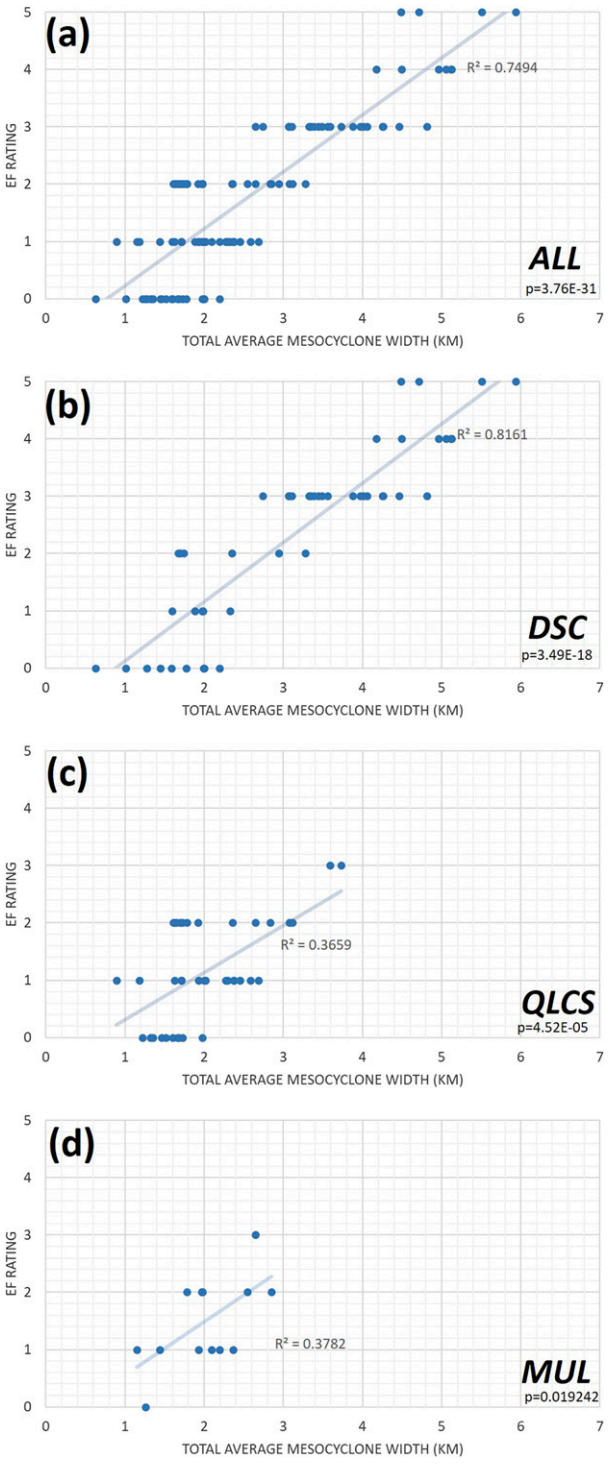

FIG. 3. Scatterplot showing the linear relationship between the total average pretornadic mesocyclone width (km) and the EF rating of the resultant tornado for (a) all cases, (b) discrete supercell (DSC) cases, (c) quasi-linear convective system (QLCS) cases, and (d) multicell (MUL) cases.

weaker (EF0–EF2) and stronger (EF3–EF5) tornadoes for all cases (Fig. 4a) and DSC cases (Fig. 4b). For QLCS and MUL cases, the more substantial overlap in pretornadic mesocyclone widths for EF0–EF2 tornadoes is consistent with the weaker relationship seen in the regression analysis (Figs. 4c,d); although there are only two QLCS EF3 tornadoes in this dataset, pretornadic mesocyclone widths for EF3 tornadoes are also separated from those associated with the EF0–EF2 cases that had narrower widths less than 3 km (Fig. 4c).

A comparison of the time-averaged and peak pretornadic mesocyclone width at each of the three lowest radar elevation angles further supports the relationship between wide mesocyclones and strong tornadoes. (The peak pretornadic mesocyclone width is the maximum over all of the analysis times during the lifetime of the pretornadic mesocyclone.) For all cases, there is a similar relationship between the EF rating and both the average and maximum pretornadic mesocyclone width across all elevation angles (Fig. 5a and Fig. 6a). A stronger relationship is shown for all elevation angles for both the average and maximum pretornadic mesocyclone width for DSC cases (Figs. 5b and 6b). For QLCS (and MUL) cases the relationship is weaker for all elevation angles, particularly the highest of the three (Figs. 5c,d and 6c,d). This may be due to the shallow, more diffuse, and shorter-lived nature of QLCS mesocyclones (e.g., Trapp et al. 1999; Atkins et al. 2004). Indeed, in this dataset, the average lifetime of the pretornadic mesocyclone was 19 min for DSC cases and 10 min for QLCS cases.

Thus far, EF rating has been used to explore the relationship between the pretornadic mesocyclone width and tornado intensity, but in light of the potential biases in damage-based ratings, the peak tornadic ΔV was also analyzed here to provide an independent measure of tornado intensity. Figure 7 shows that the linear relationship between the total average mesocyclone width and the peak tornadic ΔV ($R^2 = 0.59$) is comparable to that between total average mesocyclone width and EF rating, which provides further confidence in this general relationship. (The peak tornadic ΔV is the maximum over all the analysis times during the lifetime of the tornado.) As an aside, the strong linear relationship ($R^2 = 0.63$) between EF rating and peak tornado ΔV across all cases (Fig. 8) helps explain the relative agreement between the analyses in Figs. 3 and 7, and also supports efforts introduced by Toth et al. (2013), Kingfield and LaDue (2015), and Thompson et al. (2017) to use operational weather radar to estimate tornado intensity. This relative agreement between EF rating and the peak tornadic ΔV across all cases can also be viewed through a box-and-whisker plot (Fig. S2). When

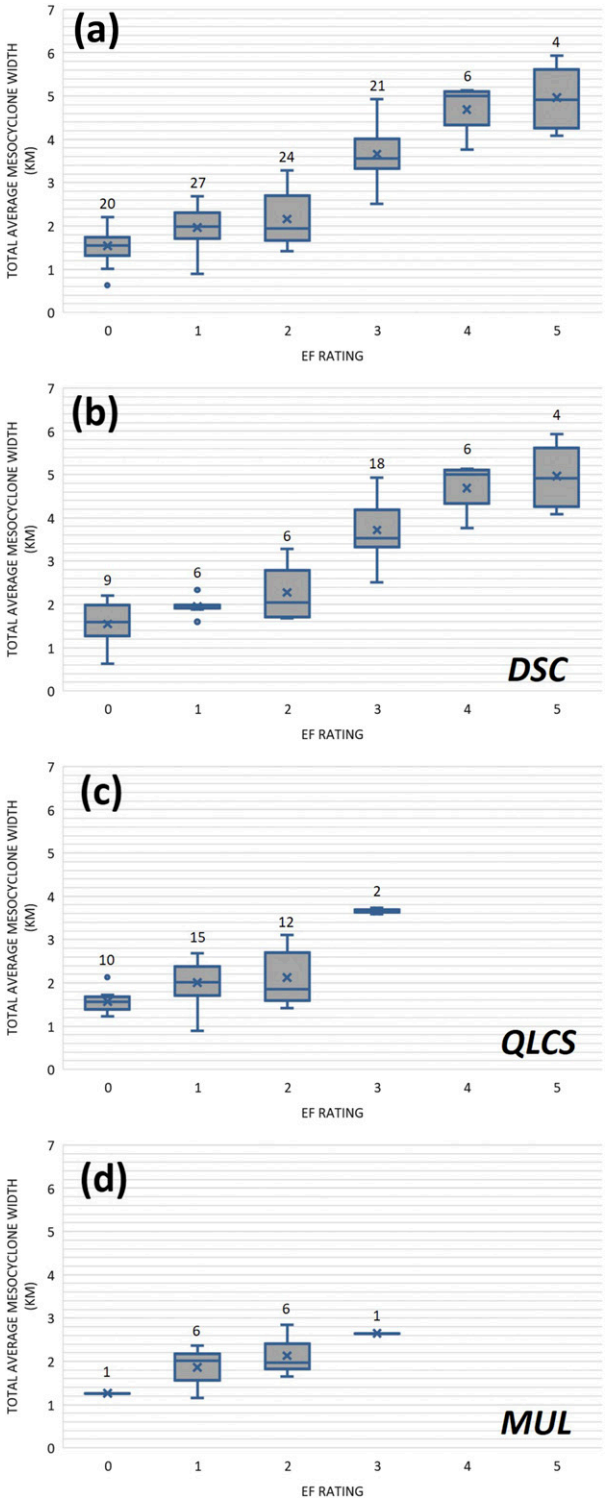

FIG. 4. Box-and-whisker plot showing the relationship between the total average pretornadic mesocyclone width (km) EF rating of the resultant tornado for (a) all cases, (b) DSC cases, (c) QLCS cases, and (d) MUL cases. The mean is represented by the × and the median by the bar. The top and bottom of the box represent the third and first quartiles with exclusive medians, respectively, and the top and bottom whiskers represent the minimum and maximum values, respectively.

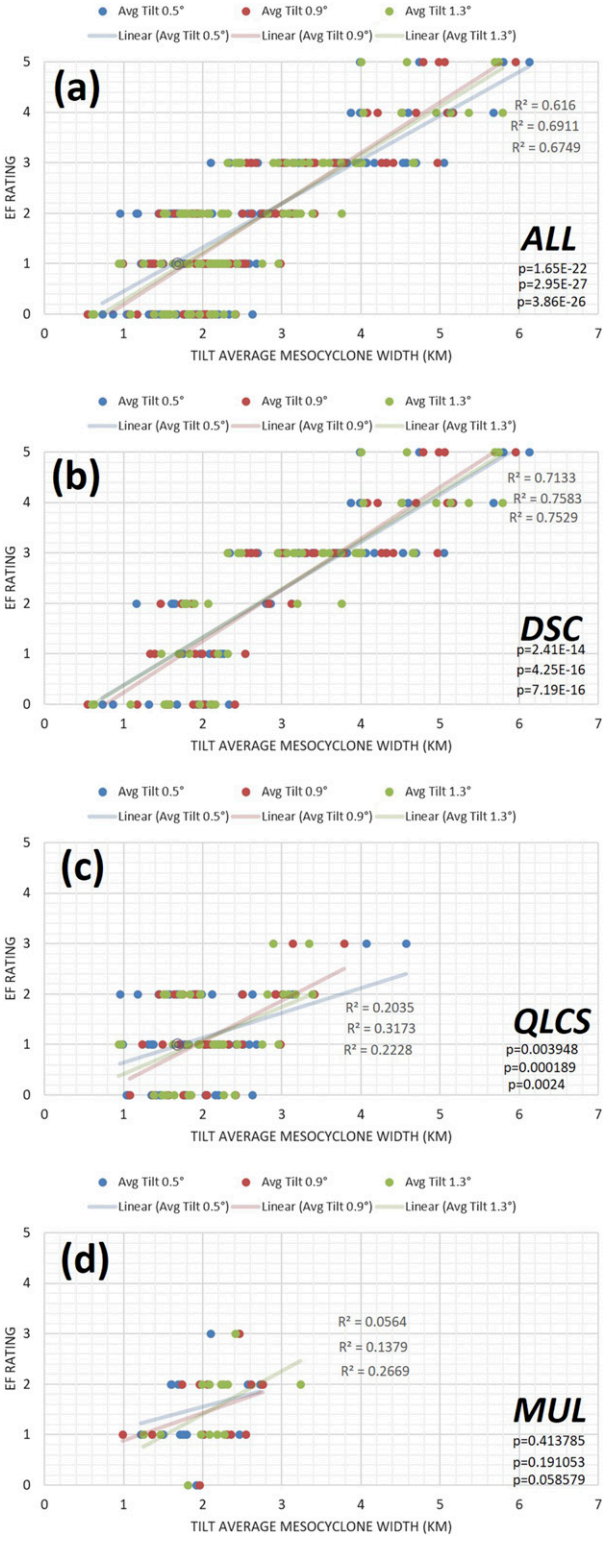

FIG. 5. Scatterplot showing the linear relationship between the total average pretornadic mesocyclone width (km) at each elevation angle (0.5°, 0.9°, and 1.3°) and the EF rating of the resultant tornado for (a) all cases, (b) DSC cases, (c) QLCS cases, and (d) MUL cases. The R^2 and p values are listed from lowest to highest tilt.

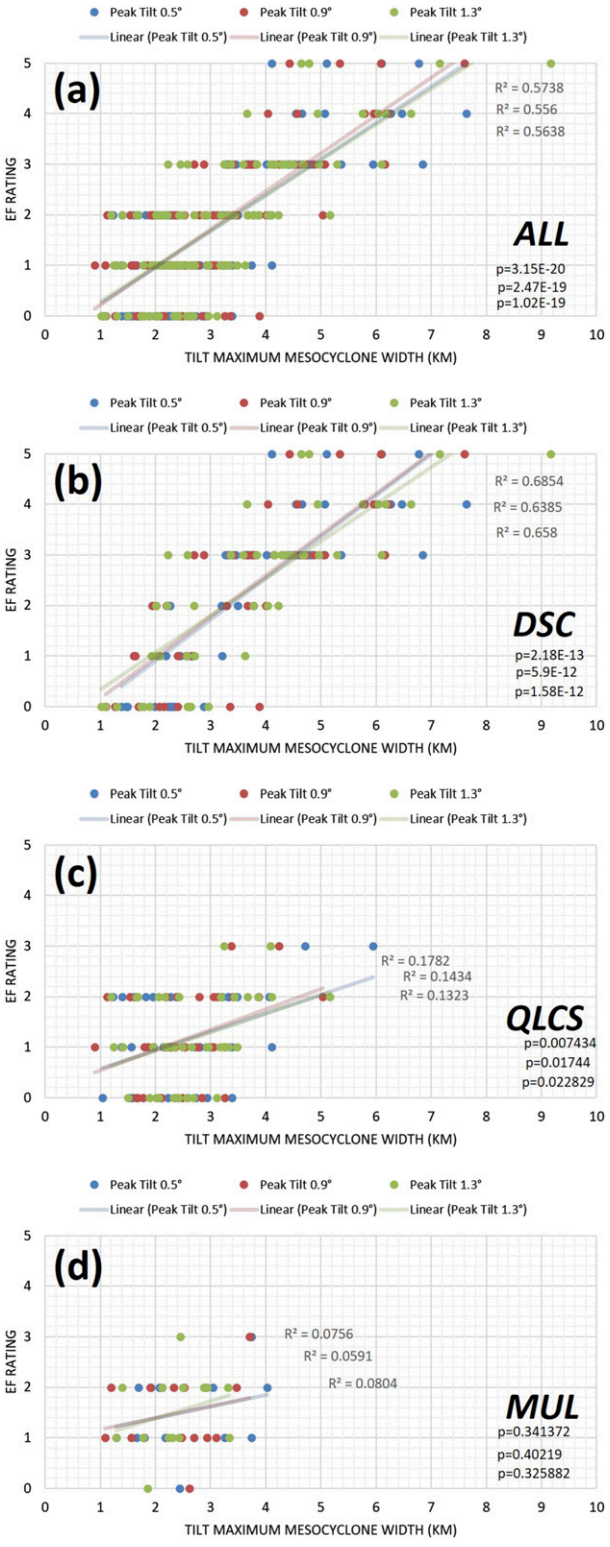

FIG. 6. As in Fig. 5, but showing the linear relationship between the maximum pretornadic mesocyclone width (km) at each elevation angle and the EF rating of the resultant tornado. The R^2 and p values are listed from lowest to highest tilt.

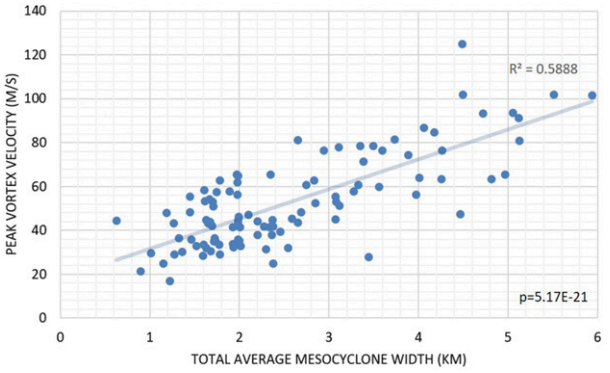

FIG. 7. Scatterplot showing the linear relationship between the peak intensity of the tornadic vortex (differential velocity; m s^{-1}) and the total average pretornadic mesocyclone width (km) for all cases.

the maximum estimated tornadic wind speed from damage assessments is used in place of EF rating, the strong linear relationship between higher damage rated tornadoes and the peak tornadic ΔV remains ($R^2 = 0.64$, Fig. S3). The substantial overlap of tornadic ΔVs in Fig. 8 across EF0–EF2 tornadoes may partially be due to the biases and inaccuracies of EF ratings for weaker tornadoes, including a lack of damage indicators.

It is possible that the ΔV as well as the mesocyclone-width analyses are sensitive to the radar range, specifically to the beam broadening with increasing range, the change of positioning of the vortex center relative to the radar beam center, and the increase in relative beam heights with range, which in turn affects the height of the vortex sampled (e.g., Wood and Brown 1997). In terms of the latter range dependency, we note for example, that for a storm 15 km from the radar, the beam height at 1.3° elevation angle is approximately 400 m AGL, and the change in height between the three lowest tilts considered here is about 100 m. For a storm about 80 km from the radar, the beam height at 1.3° elevation angle is approximately 2400 m AGL, and the change in height between the three lowest tilts is roughly 600 m. To explore the effect of range on our results, we first performed a linear regression between the total average pretornadic mesocyclone width and radar range at the time of tornadogenesis (not shown), and found only a very weak relationship ($R^2 = 0.14$). We also performed a linear regression between the total average pretornadic mesocyclone width and the 0.5° beam height (not shown), and likewise found only a very weak relationship ($R^2 = 0.16$). Both analyses suggest a limited negative impact of radar range on the key results of the study. Next, we subdivided the cases by range into three groups: 0–35-km range (31 cases), 36–70-km range (43 cases), and 71–100-km range

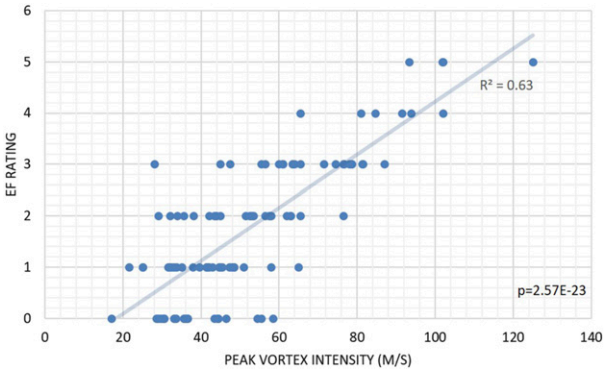

FIG. 8. Scatterplot showing the linear relationship between the peak intensity of the tornadic vortex (differential velocity; m s^{-1}) and the EF rating of the resultant tornado for all cases.

(28 cases). We found no reduction in the linear relationship between EF rating and peak tornado ΔV across these three range groupings (not shown). In terms of pretornadic mesocyclone width versus EF rating, when the total average pretornadic mesocyclone width is used, we found that the first two groups have slightly weaker linear relationships relative to that of the third group ($R^2 = 0.72$, $R^2 = 0.71$, $R^2 = 0.79$, respectively; Fig. 9). This comparatively stronger relationship at farther radar ranges is also found across the three lowest elevation angles when the peak pretornadic mesocyclone width is compared to the total average pretornadic mesocyclone width (Fig. 10), perhaps suggesting the relative importance of pretornadic mesocyclone width in the midlevels of the storm (see T17). Because the average pretornadic mesocyclone width at each elevation compares well to the total average pretornadic mesocyclone width, but with stronger relationships at farther ranges (Fig. 11), it appears that the pretornadic mesocyclone width does not vary across a large depth of the storm throughout its life cycle. Thus, if a pretornadic mesocyclone is wide in its lowest levels, it should also be wide at higher levels, as was argued on physical grounds by T17.

An open question at this point is whether the time variability of mesocyclone width during the pretornadic period is sufficiently low so as to provide a reliable indicator of tornado intensity, as hypothesized. This question was addressed in part by comparing the maximum pretornadic mesocyclone width at each of the three elevation angles to the total average mesocyclone width. As shown by Fig. 12, the linear relationship between these two variables is strong across all cases and each elevation angle. The standard deviation of the mesocyclone width was also analyzed and compared to the total average mesocyclone width for all of the cases

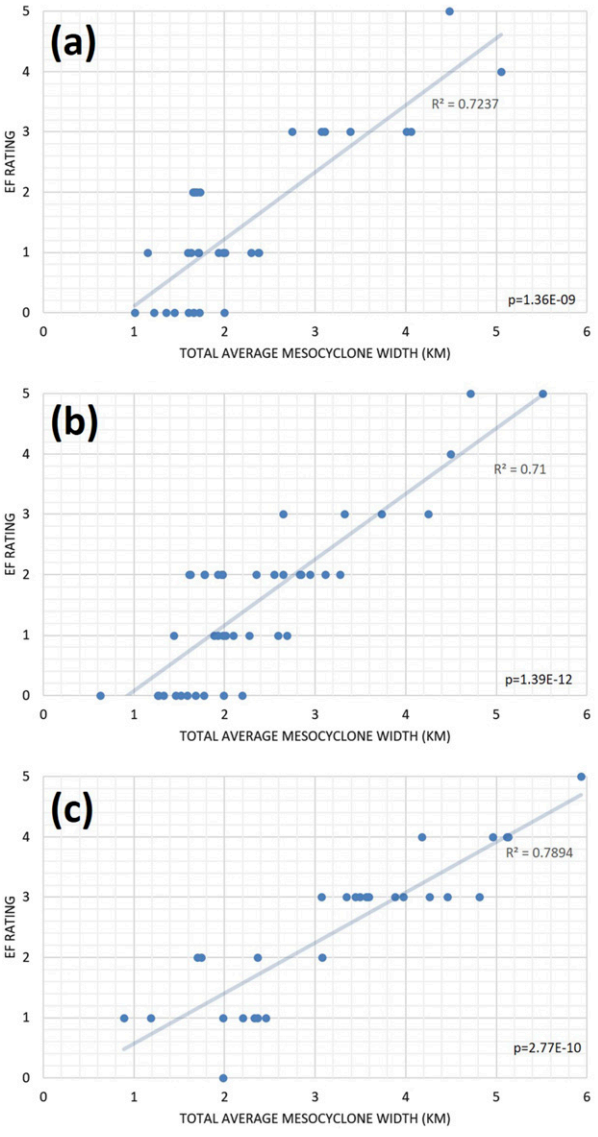

FIG. 9. Scatterplot showing the linear relationship between the average pretornadic mesocyclone width (km) and the EF rating of the resultant tornado for all cases with a radar range of (a) 0–35, (b) 36–70, and (c) 71–100 km.

individually. Although some of the cases exhibit standard deviations that are more than 50% of the mean, the linear relationship between these two variables is weak across all cases ($R^2 = 0.20$) (Fig. 13). In other words, the time variability of a pretornadic wide mesocyclone is comparable to that of a narrow mesocyclone. Both of these analyses are interpreted to mean that a mesocyclone that is wide (narrow) at some point during its pretornadic period generally remains a wide (narrow) mesocyclone.

The pretornadic mesocyclones did undergo some contraction just prior to tornadogenesis, however. There

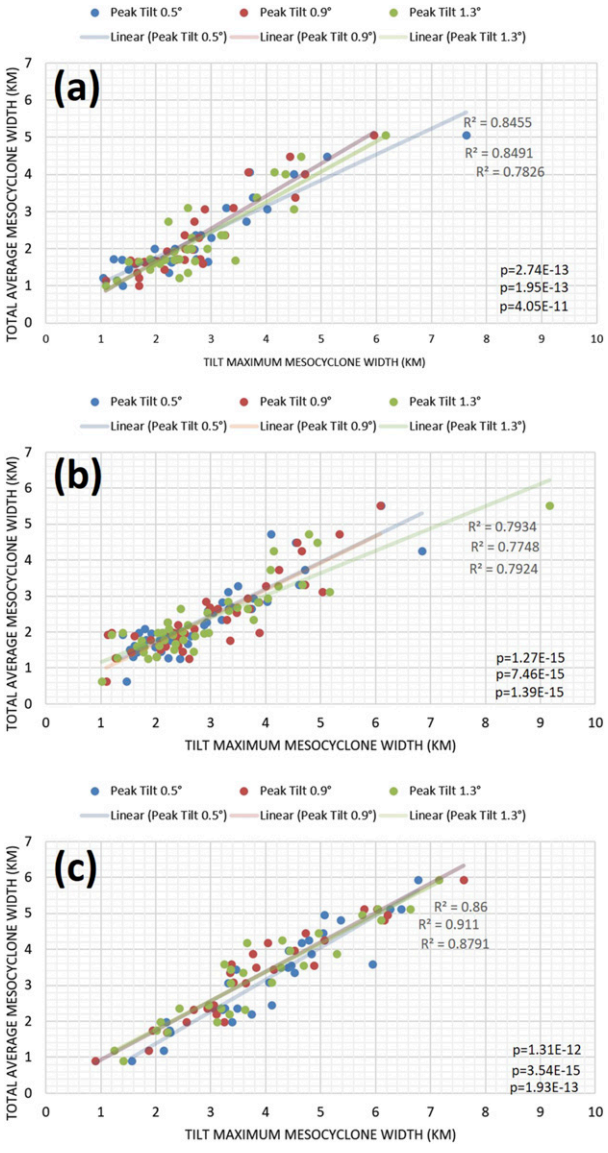

FIG. 10. Scatterplot showing the linear relationship between the peak pretornadic mesocyclone width at each elevation angle and the total average pretornadic mesocyclone width (km) for cases with a radar range of (a) 0–35, (b) 36–70, and (c) 71–100 km. The R^2 and p values are listed from lowest to highest tilt.

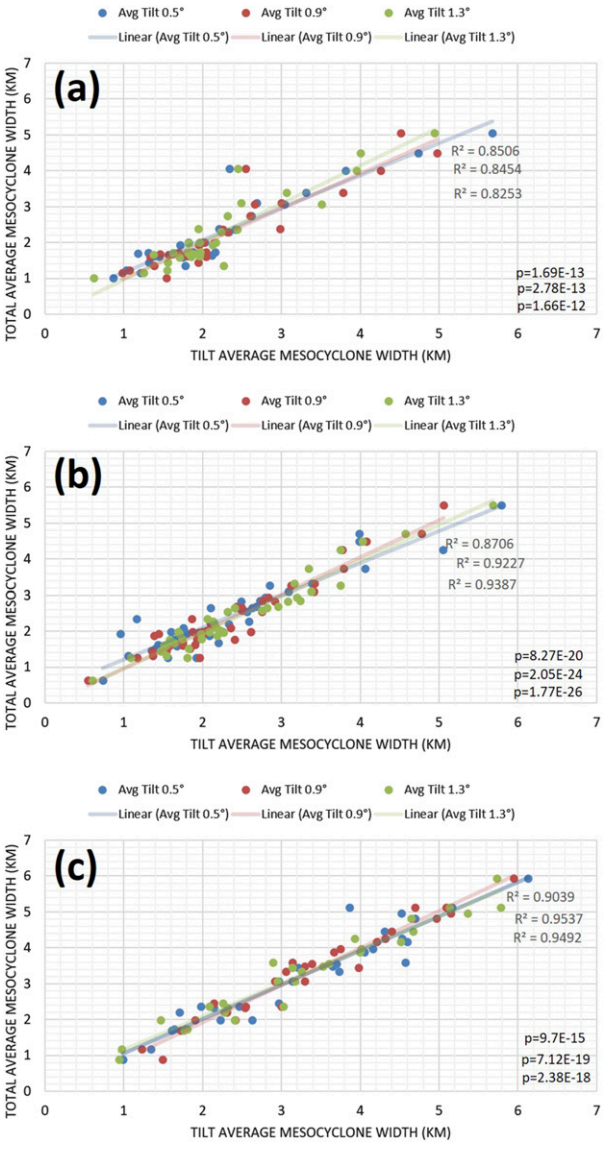

FIG. 11. As in Fig. 10, but showing the linear relationship between the average pretornadic mesocyclone width at each elevation angle and the total average pretornadic mesocyclone width (km). The R^2 and p values are listed from lowest to highest tilt.

were 53 out of 102 cases that experienced a decrease in the total average pretornadic mesocyclone width of at least 5% during the two volume scans prior to tornadogenesis; at the lowest elevation angle, 60 out of the 102 cases experienced this decrease in the total average pretornadic mesocyclone width. A change in the pretornadic mesocyclone ΔV was also noted: 67 out of 102 cases experienced an increase in the average mesocyclone ΔV of at least $5\,\mathrm{m\,s^{-1}}$ during the two volume scans prior to tornadogenesis. Specifically, the majority of tornadoes rated EF3 and greater were associated with mesocyclones that narrowed and strengthened just prior to tornadogenesis. This supports the idea that a pretornadic mesocyclone that shows an increase in ΔV and a decrease in width immediately prior to tornadogenesis may be more likely to produce a tornado, specifically a potentially strong tornado. Previous work describing fundamental tornado and supercell dynamics (e.g., Davies-Jones 2015) supports convergence and narrowing of the pretornadic circulation, and an increase in the differential velocity of the pretornadic mesocyclone, and a narrowing and intensifying

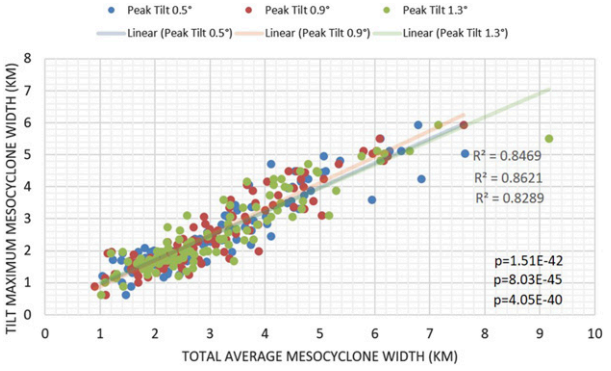

FIG. 12. Scatterplot showing the linear relationship between the peak pretornadic mesocyclone width at each elevation angle and the total average pretornadic mesocyclone width (km) at each elevation angle for all cases. The R^2 and p values are listed from lowest to highest tilt.

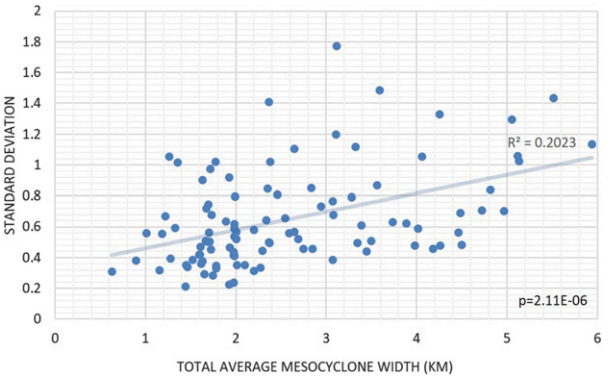

FIG. 13. Scatterplot showing the linear relationship between the standard deviation of the pretornadic mesocyclone width (km) and the average pretornadic mesocyclone width (km) for all cases.

of the pretornadic mesocyclone particularly for discrete, EF2+ tornado producing storms has been observed in other observational studies (Gibbs and Bowers 2019).

As just alluded to, the intensity of the pretornadic mesocyclone would appear to be another characteristic that, like width (or in addition to width), could be exploited to help anticipate tornado intensity. However, Fig. 14a reveals that the linear relationship between the peak pretornadic mesocyclone ΔV, defined as the maximum ΔV over all analysis times and tilts during the lifetime of the pretornadic mesocyclone, and EF rating for all cases is relatively weak ($R^2 = 0.42$). When the maximum estimated tornadic wind speed from damage assessments is used in place of EF rating, the weaker relationship between higher damage rated tornadoes and the peak pretornadic mesocyclone ΔV remains but is slightly higher ($R^2 = 0.45$, Fig. S4). When this relationship is explored through a box-and-whisker plot, an increase in peak pretornadic mesocyclone ΔV with increasing EF rating is apparent, but so also is the substantial overlap across each EF rating, particularly with weaker EF-rated tornadoes (Fig. 14d). If the peak pretornadic mesocyclone ΔV at each tilt is averaged and compared to EF rating, the linear relationship remains weak ($R^2 = 0.39$) (Fig. 14b). Finally, if the maximum pretornadic mesocyclone ΔV at each elevation angle is compared to EF rating, the linear relationship improves somewhat, especially at elevation angle 3 ($R^2 = 0.40$) (Fig. 14c), but still is comparatively weak. Although the EF4–5 cases tended to be associated with the strongest pretornadic mesocyclones, the conclusion from this analysis is that relatively higher EF-rated tornadoes do not necessarily tend to be associated with more intense pretornadic mesocyclones; this basic conclusion applies across all convective modes (not shown).

This analysis of pretornadic mesocyclone ΔV can also be extended to provide a comparison between mesocyclone width and intensity. Figure 15 reveals that the overall peak pretornadic mesocyclone ΔV had a weak linear relationship with total average pretornadic mesocyclone width ($R^2 = 0.37$); if the peak pretornadic mesocyclone ΔV at each of the three elevation angles is averaged and compared with the total average pretornadic mesocyclone width, there is a similarly weak relationship ($R^2 = 0.36$) (Fig. 16). The conclusion here is that the widest pretornadic mesocyclones are not necessarily the strongest pretornadic mesocyclones, and vice versa. This result is consistent with the conservation of circulation argument in T17, which shows how a given circulation can result from different plausible mesocyclonic widths and rotational velocities, such as a wider mesocyclone with a weaker rotational velocity or a narrower mesocyclone with a stronger rotational velocity.

The results of Brooks (2004) and T17 imply that the tornado damage width should also relate to the pretornadic mesocyclone width. Analysis of the damage path information provided in the NOAA Storm Database shows that the smallest pretornadic mesocyclone widths of around 1 km tended to be associated with the smallest tornado damage widths. At the other extreme, the largest pretornadic mesocyclone widths of around 5 km tended to be associated with larger tornado damage widths. However, over all cases, the relationship between the tornado damage width and the total average pretornadic mesocyclone width is weak (Fig. 17a, $R^2 = 0.36$). This is reflected the least in DSC cases (Fig. 17b, $R^2 = 0.43$), but particularly in MUL cases (Fig. 17c, $R^2 = 0.0004$), as well as QLCS cases (Fig. 17d, $R^2 = 0.25$). To test whether a large range of widths for

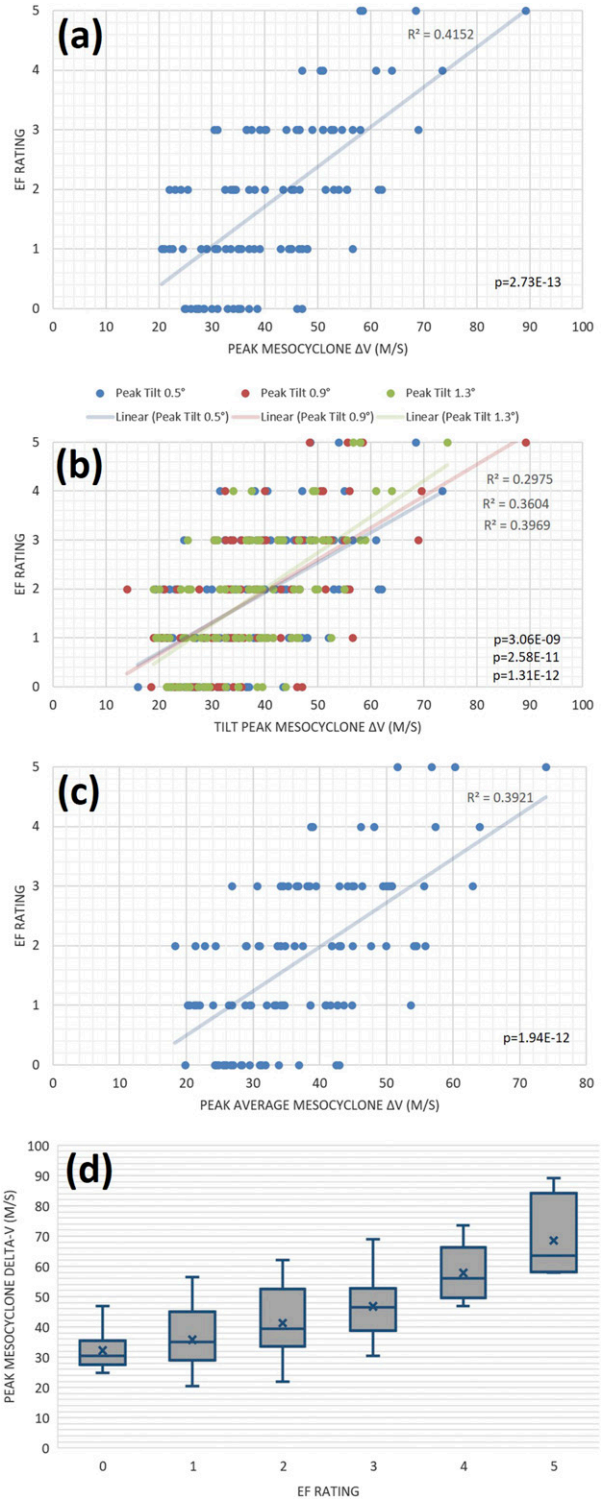

FIG. 14. Scatterplot showing the linear relationship between the EF rating of the resultant tornado and (a) peak pretornadic mesocyclone intensity (differential velocity; $m\,s^{-1}$), (b) peak average pretornadic mesocyclone intensity (differential velocity; $m\,s^{-1}$), and (c) peak pretornadic mesocyclone intensity (differential velocity; $m\,s^{-1}$) at each elevation angle for all cases. The R^2 and p values are listed from lowest to highest tilt. (d) A box-and-whisker plot as in Fig. 4, but now showing the relationship between the peak pretornadic mesocyclone intensity (differential velocity; $m\,s^{-1}$) and the EF rating of the resultant tornado.

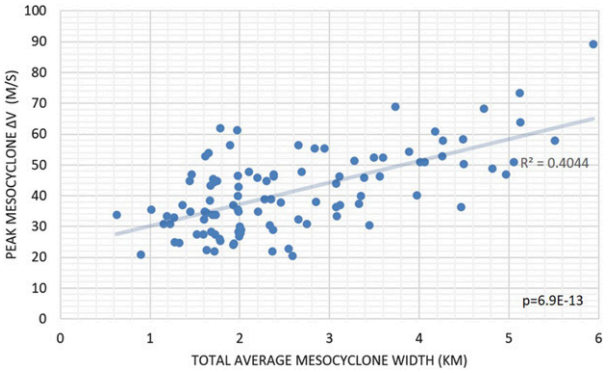

FIG. 15. Scatterplot showing the linear relationship between the peak pretornadic mesocyclone intensity (differential velocity; $m\,s^{-1}$) and the average pretornadic mesocyclone width (km) for all cases.

weaker tornadoes was impacting these results, EF0 and EF1 tornadoes were removed. This test was motivated by the weaker and narrower nature of QLCS tornadoes and the tendency of their damage to be aliased into straight line wind damage (Trapp et al. 2005b; Skow and Cogil 2017). There was little to no impact on the relationship between tornado damage width and total average mesocyclone width, though. Based on this analysis, the pretornadic mesocyclone width does not appear to accurately anticipate tornado damage width, implying that the presence of a wide pretornadic mesocyclone does not mean that, if a tornado forms, it will be wide. The overall poor relationship between tornado damage width and total average mesocyclone width, especially with QLCS events, may be partially due to the insufficiency of damage indicators or lack of damage indicators (e.g., Edwards et al. 2013; Snyder and Bluestein 2014).

The relationship between tornado pathlength and the total average pretornadic mesocyclone width was also weak (Fig. 18a, $R^2 = 0.32$) across all cases. Although the longest-track tornadoes from DSC events were associated with wider pretornadic mesocyclones, overall a weak relationship was found for each of the convective mode categories (Figs. 18b–d), with a large spread of tornado pathlengths associated with both relatively wide and narrow mesocyclones, especially for QLCS events. Thus, the presence of a wide or narrow pretornadic mesocyclone does not appear to

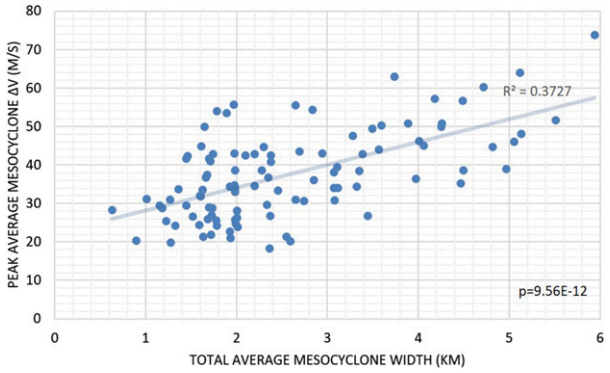

FIG. 16. Scatterplot showing the linear relationship between the peak average intensity of the pretornadic mesocyclone (differential velocity; $m\,s^{-1}$) and the total average width of the pretornadic mesocyclone (km) for all cases.

accurately anticipate the likelihood of a long- or short-track tornado.

Finally, because our study was motivated in part by the desire to better anticipate tornado intensity within the southeastern United States, the previous analyses were repeated for only those cases located within the states of South Carolina, Georgia, Florida, Alabama, Mississippi, Louisiana, Arkansas, and Tennessee. Over this subdomain, the linear relationship between the total average pretornadic mesocyclone width and EF rating is slightly reduced ($R^2 = 0.70$) relative to that over all cases ($R^2 = 0.75$) yet still strong. The relationships for DSC cases were slightly higher ($R^2 = 0.85$) and the relationships for QLCS cases were slightly weaker ($R^2 = 0.31$) compared to those over all cases ($R^2 = 0.82$ and $R^2 = 0.37$, respectively). This result suggests that the observational realization of the T17 hypothesis is not geographically constrained.

4. Operational application

The preceding analyses of radar characteristics of pretornadic mesocyclones were based on the knowledge that a tornado had occurred for each of the cases. *Thus, the results presented herein should not be interpreted as a means to anticipate tornado formation.* Rather, the results should be used in tandem with environmental information (e.g., Smith et al. 2015) as an additional means to anticipate the likely tornado intensity/damage, given tornado formation.

Specifically, a radar-based diagnosis of a wide mesocyclone appears to increase the likelihood of a higher EF-rated tornado, particularly for tornadoes forming within supercell thunderstorms. More specifically, a pretornadic mesocyclone with a width greater than

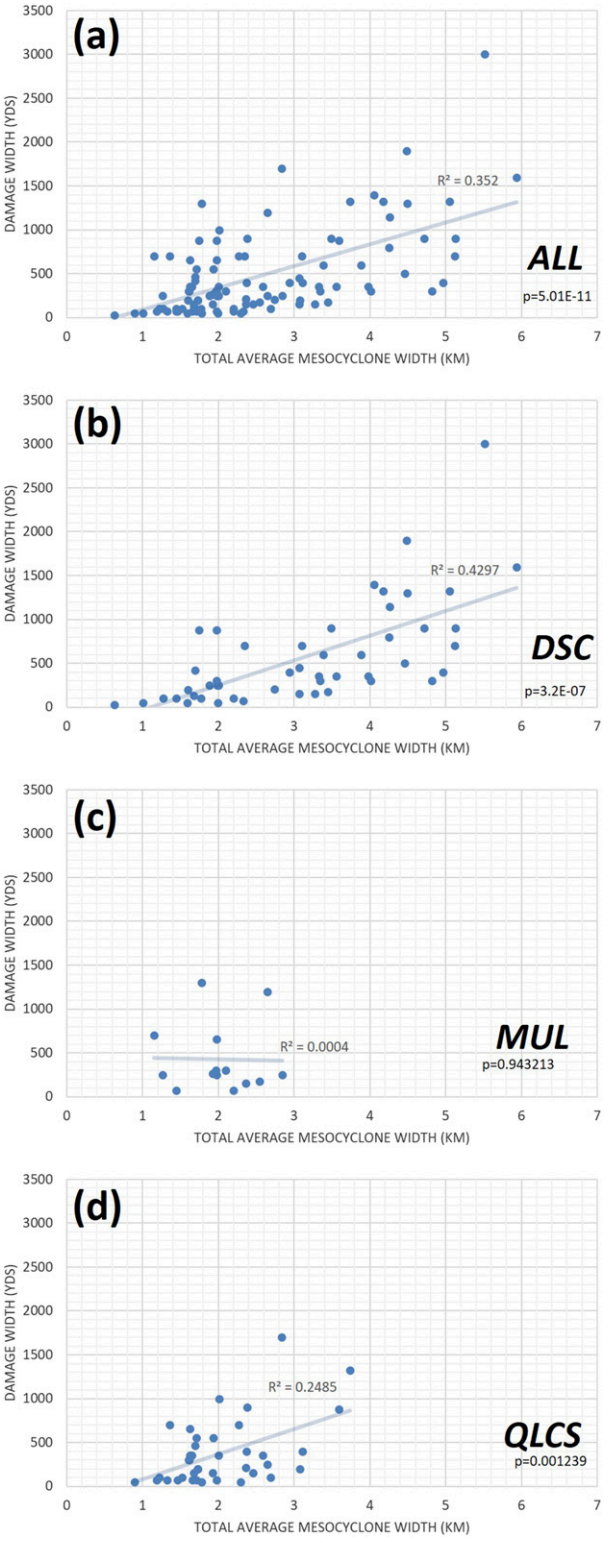

FIG. 17. Scatterplot showing the linear relationship between the damage width of the resultant tornado (yards) and the total average pretornadic mesocyclone width (km) (a) all cases, (b) DSC cases, (c) MUL cases, and (d) QLCS cases.

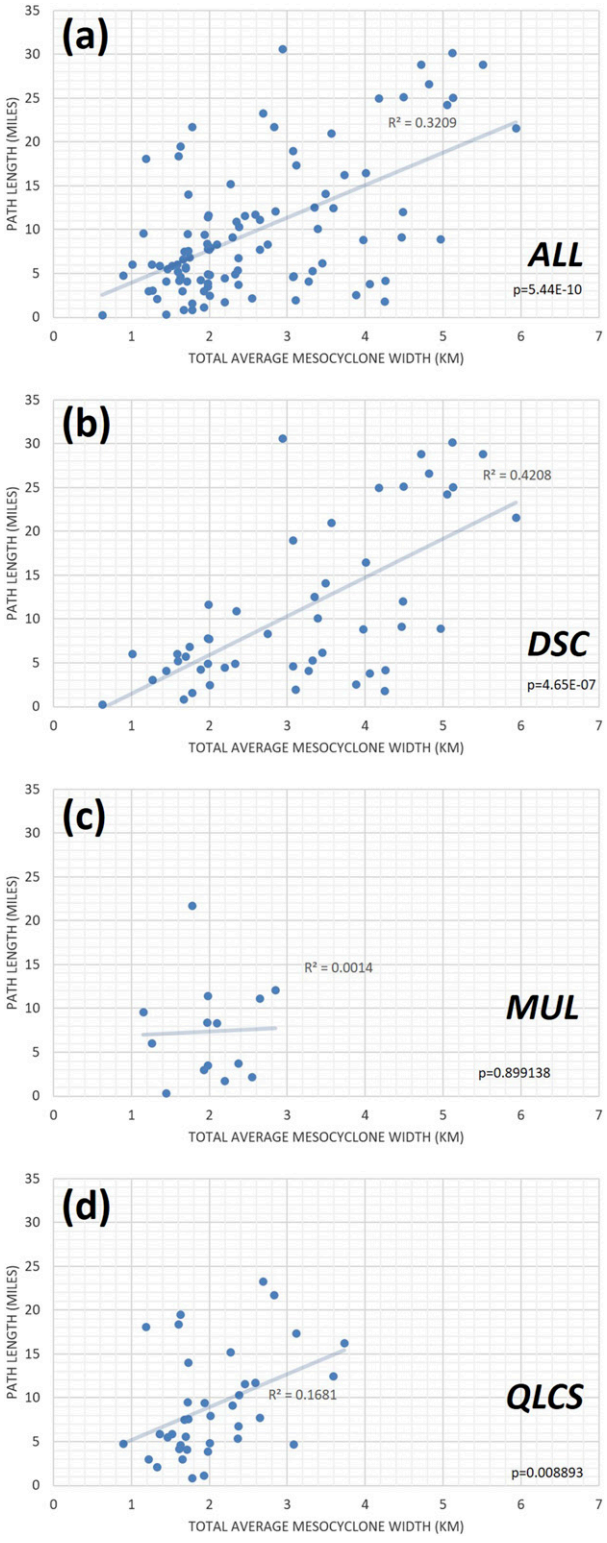

FIG. 18. As in Fig. 17, but showing the linear relationship between the pathlength of the resultant tornado (miles) and the total average pretornadic mesocyclone width (km).

3 km (less than 1 km) appears more likely to generate tornadoes rated EF3 and higher (EF1 and less). Based on our analyses, the width characterization (i.e., of "wide" versus "narrow") should not change significantly in time leading up to tornadogenesis, thus making this characterization a relatively more reliable indicator than mesocyclone intensity. Our analyses also show that it should not be expected that a wide (narrow) mesocyclone will necessarily be a strong (weak) mesocyclone, nor should it be expected that stronger pretornadic mesocyclones will necessarily produce higher EF-rated tornadoes. In addition, the width characterization should not be greatly impacted by radar range, provided that the mesocyclone is within 100 km from the radar. Both findings are consistent across all convective modes. On the other hand, the pretornadic mesocyclone width does not appear to be operationally useful for anticipating the potential for tornado damage-path width or length. This finding is consistent across all modes, but merits future study using well constrained damage surveys.

5. Summary, conclusions, and future work

Operational radar data and tornado reports were used herein to test the generality of the Trapp et al. (2017) hypothesis that wide, intense tornadoes should form more readily out of wide, rotating updrafts. A new radar dataset was assembled that focuses explicitly on the *pretornadic* characteristics of the mesocyclone, which allowed for the elimination of the effects of the tornado itself on the mesocyclone characteristics. GR2Analyst was used to manually analyze 102 tornadic events during the period 27 April 2011–1 May 2019. The corresponding tornadoes had damage (EF) ratings ranging from EF0 to EF5, and all were within 100 km of a WSR-88D. Several linear regression analyses were completed comparing characteristics of the pretornadic mesocyclone to tornado intensity. A key finding is that the linear regression between the EF rating of the tornado and the mean, pretornadic width of the mesocyclone for all cases yields a coefficient of determination (R^2) value of 0.75. This linear relationship is higher for DSC (supercell) cases ($R^2 = 0.82$), and lower for QLCS cases ($R^2 = 0.37$). Overall, we have found that pretornadic mesocyclone width tends to be a persistent, relatively time-invariant characteristic that is a good predictor of potential tornado intensity. In contrast, the pretornadic mesocyclone intensity (differential velocity) tends to exhibit considerable time variability, and thus would offer less reliability in anticipating tornado intensity.

In our future work, the environmental characteristics of each case will be analyzed and compared to pretornadic mesocyclone characteristics. This will be done to better understand the environmental controls on the pretornadic mesocyclone width and intensity and any dependence of the pretornadic mesocyclone on convective mode. There will also be further analysis of the pretornadic mesocyclone, and its coevolution with updraft properties revealed at cloud top through overshooting top area (Marion et al. 2019), to explore for the presence of any operationally useful trends which would allude to a potential tornado intensity or tornadogenesis. In addition, case simulations using the Weather Research and Forecasting Model will be used to further explore the relationship between the pretornadic mesocyclone and tornado intensity and any potential environmental controls.

Acknowledgments. This research was supported by NOAA through Award NA17OAR4590195. Julissa Einbinder performed some of the radar analyses as part of her undergraduate capstone research project at the University of Illinois. Helpful comments on the methodology and results were provided by Geoff Marion, Jake Mulholland, and Devin Chehak. Feedback on the overall research was also provided by Steve Nelson (NWS Peachtree City), Ray Wolf (NWS Quad Cities), and Pat Spoden (NWS Paducah). Suggestions by the three anonymous reviewers helped improve and refine the manuscript.

REFERENCES

Ashley, W. S., 2007: Spatial and temporal analysis of tornado fatalities in the United States: 1880–2005. *Wea. Forecasting*, **22**, 1214–1228, https://doi.org/10.1175/2007WAF2007004.1.

Atkins, N. T., J. M. Arnott, R. W. Przybylinski, R. A. Wolf, and B. D. Ketcham, 2004: Vortex structure and evolution within bow echoes. Part I: Single-Doppler and damage analysis of the 29 June 1998 derecho. *Mon. Wea. Rev.*, **132**, 2224–2242, https://doi.org/10.1175/1520-0493(2004)132<2224:VSAEWB>2.0.CO;2.

Brooks, H. E., 2004: On the relationship of tornado path length and width to intensity. *Wea. Forecasting*, **19**, 310–319, https://doi.org/10.1175/1520-0434(2004)019<0310:OTROTP>2.0.CO;2.

Carbone, R. E., 1983: A severe frontal rainband. Part II: Tornado parent vortex circulation. *J. Atmos. Sci.*, **40**, 2639–2654, https://doi.org/10.1175/1520-0469(1983)040<2639:ASFRPI>2.0.CO;2.

Cohen, A. E., J. B. Cohen, R. L. Thompson, and B. T. Smith, 2018: Simulating tornado probability and tornado wind speed based on statistical models. *Wea. Forecasting*, **33**, 1099–1108, https://doi.org/10.1175/WAF-D-17-0170.1.

Conrad, D. M., and K. R. Knupp, 2019: Doppler radar observations of horizontal shearing instability in quasi-linear convective systems. *Mon. Wea. Rev.*, **147**, 1297–1318, https://doi.org/10.1175/MWR-D-18-0257.1.

Davies-Jones, R., 2015: A review of supercell and tornado dynamics. *Atmos. Res.*, **158–159**, 274–291, https://doi.org/10.1016/j.atmosres.2014.04.007.

Davis, J. M., and M. D. Parker, 2014: Radar climatology of tornadic and nontornadic vortices in high-shear, low-CAPE environments in the mid-Atlantic and Southeastern United States. *Wea. Forecasting*, **29**, 828–853, https://doi.org/10.1175/WAF-D-13-00127.1.

Edwards, R., J. G. LaDue, J. T. Ferree, K. Scharfenberg, C. Maier, and W. L. Coulbourne, 2013: Tornado intensity estimation: Past, present, and future. *Bull. Amer. Meteor. Soc.*, **94**, 641–653, https://doi.org/10.1175/BAMS-D-11-00006.1.

Gibbs, J. G., and B. R. Bowers, 2019: Techniques and thresholds of significance for using WSR-88D velocity data to anticipate significant tornadoes. *J. Oper. Meteor.*, **7**, 117–137, https://doi.org/10.15191/NWAJOM.2019.0709.

Kingfield, D. M., and J. G. LaDue, 2015: The relationship between automated low-level velocity calculations from the WSR-88D and maximum tornado intensity determined from damage surveys. *Wea. Forecasting*, **30**, 1125–1139, https://doi.org/10.1175/WAF-D-14-00096.1.

Kirkpatrick, C., E. W. McCaul Jr, and C. Cohen, 2009: Variability of updraft and downdraft characteristics in a large parameter space study of convective storms. *Mon. Wea. Rev.*, **137**, 1550–1561, https://doi.org/10.1175/2008MWR2703.1.

Lee, B. D., and R. B. Wilhelmson, 1997: The numerical simulation of non-supercell tornadogenesis. Part I: Initiation and evolution of pretornadic misocyclone circulations along a dry outflow boundary. *J. Atmos. Sci.*, **54**, 32–60, https://doi.org/10.1175/1520-0469(1997)054<0032:TNSONS>2.0.CO;2.

Marion, G. R., R. J. Trapp, and S. W. Nesbitt, 2019: Using overshooting top area to discriminate potential for large, intense tornadoes. *Geophys. Res. Lett.*, **46**, 12 520–12 526, https://doi.org/10.1029/2019GL084099.

Markowski, P. M., and Y. P. Richardson, 2009: Tornadogenesis: Our current understanding, forecasting considerations, and questions to guide future research. *Atmos. Res.*, **93**, 3–10, https://doi.org/10.1016/j.atmosres.2008.09.015.

NOAA/NCEI/NESDIS, 2014: NCEI storm events database, version 3.0. NCDC, accessed 28 April 2019, https://www.ncdc.noaa.gov/stormevents.

Parker, M. D., B. S. Borchardt, R. L. Miller, and C. L. Ziegler, 2019: Simulated evolution and severe wind production by the 25–26 June 2015 nocturnal MCS from PECAN. *Mon. Wea. Rev.*, **148**, 183–209, https://doi.org/10.1175/MWR-D-19-0072.1.

Skow, K. D., and C. Cogil, 2017: A high-resolution aerial survey and radar analysis of quasi-linear convective system surface vortex damage paths from 31 August 2014. *Wea. Forecasting*, **32**, 441–467, https://doi.org/10.1175/WAF-D-16-0136.1.

Smith, B. T., R. L. Thompson, J. S. Grams, C. Broyles, and H. E. Brooks, 2012: Convective modes for significant severe thunderstorms in the contiguous United States. Part I: Storm classification and climatology. *Wea. Forecasting*, **27**, 1114–1135, https://doi.org/10.1175/WAF-D-11-00115.1.

——, ——, A. R. Dean, and P. T. Marsh, 2015: Diagnosing the conditional probability of tornado damage rating using environmental and radar attributes. *Wea. Forecasting*, **30**, 914–932, https://doi.org/10.1175/WAF-D-14-00122.1.

Snyder, J. C., and H. B. Bluestein, 2014: Some considerations for the use of high-resolution mobile radar data in tornado intensity determination. *Wea. Forecasting*, **29**, 799–827, https://doi.org/10.1175/WAF-D-14-00026.1.

Thompson, R. L., and Coauthors, 2017: Tornado damage rating probabilities derived from WSR-88D data. *Wea. Forecasting*, **32**, 1509–1528, https://doi.org/10.1175/WAF-D-17-0004.1.

Toth, M., R. J. Trapp, J. Wurman, and K. A. Kosiba, 2013: Comparison of mobile-radar measurements of tornado intensity with corresponding WSR-88D measurements. *Wea. Forecasting*, **28**, 418–426, https://doi.org/10.1175/WAF-D-12-00019.1.

Trapp, R. J., 2013: *Mesoscale-Convective Processes in the Atmosphere*. Cambridge University Press, 346 pp.

——, and M. L. Weisman, 2003: Low-level mesovortices within squall lines and bow echoes. Part II: Their genesis and implications. *Mon. Wea. Rev.*, **131**, 2804–2823, https://doi.org/10.1175/1520-0493(2003)131<2804:LMWSLA>2.0.CO;2.

——, E. D. Mitchell, G. A. Tipton, D. W. Effertz, A. I. Watson, D. L. Andra, and M. A. Magsig, 1999: Descending and nondescending tornadic vortex signatures detected by WSR-88Ds. *Wea. Forecasting*, **14**, 625–639, https://doi.org/10.1175/1520-0434(1999)014<0625:DANTVS>2.0.CO;2.

——, G. J. Stumpf, and K. L. Manross, 2005a: A reassessment of the percentage of tornadic mesocyclones. *Wea. Forecasting*, **20**, 680–687, https://doi.org/10.1175/WAF864.1.

——, S. A. Tessendorf, E. S. Godfrey, and H. E. Brooks, 2005b: Tornadoes from squall lines and bow echoes. Part I: Climatological distribution. *Wea. Forecasting*, **20**, 23–34, https://doi.org/10.1175/WAF-835.1.

——, G. R. Marion, and S. W. Nesbitt, 2017: The regulation of tornado intensity by updraft width. *J. Atmos. Sci.*, **74**, 4199–4211, https://doi.org/10.1175/JAS-D-16-0331.1.

——, ——, and ——, 2018: Reply to ''Comments on 'The regulation of tornado intensity by updraft width.'''. *J. Atmos. Sci.*, **75**, 4057–4061, https://doi.org/10.1175/JAS-D-18-0276.1.

Wheatley, D. M., and R. J. Trapp, 2008: The effect of mesoscale heterogeneity on the genesis and structure of mesovortices within quasi-linear convective systems. *Mon. Wea. Rev.*, **136**, 4220–4241, https://doi.org/10.1175/2008MWR2294.1.

Wood, V. T., and R. A. Brown, 1997: Effects of radar sampling on single-Doppler velocity signatures of mesocyclones and tornadoes. *Wea. Forecasting*, **12**, 928–938, https://doi.org/10.1175/1520-0434(1997)012<0928:EORSOS>2.0.CO;2.